Supporting information

Electron-hopping brings lattice strain and high catalytic activity in low temperature oxidative coupling of methane in an electric field

Shuhei Ogo*[†‡], Hideaki Nakatsubo[†], Kousei Iwasaki[†], Ayaka Sato[†], Kota Murakami[†], Tomohiro Yabe[†], Atsushi Ishikawa[‡§¶], Hiromi Nakai[§], and Yasushi Sekine[†]

[†] *Department of Applied Chemistry, Waseda University, 3-4-1, Okubo, Shinjuku, Tokyo, 169-8555 Japan*

[‡] *PRESTO, Japan Science and Technology Agency (JST), 4-1-8 Honcho, Kawaguchi, Saitama 332-0012, Japan*

[§] *Department of Chemistry and Biochemistry, Waseda University, 3-4-1, Okubo, Shinjuku, Tokyo, 169-8555 Japan*

[¶] *Center for Green Research on Energy and Environmental Materials*, *National Institute of Materials Science, 1-1, Namiki, Tsukuba, Ibaraki, 305-0044 Japan*

*: Corresponding author: ogo@aoni.waseda.jp

Preparation of $Ce_2(WO_4)_3$

$Ce_2(WO_4)_3$ was prepared using an EDTA-citrate complex polymerization method, as described in previous papers.[1,2] Firstly, EDTA (Ethylenediaminetetraacetic acid; Kanto Chemical Co., Inc.) was dissolved in aqueous ammonia (28.0−30.0%; Kanto Chemical Co., Inc.), and then an aqueous solution of $Ce(NO_3)_3 \cdot 6H_2O$ (Kanto Chemical Co., Inc.) was added. Subsequently, WO_3 (Kanto Chemical Co., Inc.) was added to the solution. After 15 min of stirring at 313 K, citric acid (Kanto Chemical Co., Inc.) was added; the pH of the solution was adjusted to 10 using the aqueous ammonia with a temperature fixed to 353 K. The prepared solution was stirred at 353 K until formation of gel-like precipitate. This gel-like precipitate was pre-calcined for 3 h in a maffle furnace at 503 K under a ramping rate of 5 K min^{-1} to obtain powder primer. This Powder primer was calcined for 5 h in the maffle furnace at 1273 K under a ramping rate of 5 K min^{-1} to obtain well-crystalized $Ce_2(WO_4)_3$. The molar ratio of EDTA, citric acid, and total metal ions (Ce+W) was 1:1.5:1.

Preparations of $Ln_2(WO_4)_3$

$Ln_2(WO_4)_3$ (Ln = La, Pr, Nd, Sm, Eu, Gd, Tb, Dy) catalysts were prepared according to the published procedure.[3] Stoichiometric amounts (Ln:W = 2:3) of $Ln(NO_3)_3 \cdot 6H_2O$ (Kanto Chemical Co., Inc.) and ammonium metatungstate hydrate ($(NH_4)_6H_2W_{12}O_{40} \cdot nH_2O$, STREM CHEMICALS) were dissolved in distilled water, and then stirred at 353 K until formation of gel-like precipitate. The prepared gel-like precipitate was calcined for 12 h in the maffle furnace at 1173 K under a ramping rate of 10 K min^{-1}. The calcined sample was ground with an agate mortar at room temperature, followed by another 12 h of calcination at 1173 K to obtain well-crystalized $Ln_2(WO_4)_3$.

Preparation of $Ce_2(WO_4)_3/CeO_2$

$Ce_2(WO_4)_3/CeO_2$ catalyst containing 11.9 wt% W was prepared using an impregnation method with water as the solvent, as described in earlier reports.[4,5] An ammonium metatungstate hydrate ($(NH_4)_6H_2W_{12}O_{40}\cdot H_2O$) was used as a precursor. After impregnation, the resulting suspension was evaporated. Then the resulting solid was dried at 393 K overnight, followed by calcination for 3 h in air at 1173 K under a ramping rate of 0.5 K min^{-1}.

Table S1. Oxidative coupling of methane over $La_2(WO_4)_3$ catalyst in the electric field with various imposed currents and voltages [a]

Current / mA	Voltage / V	T_{tc} [b] / K	Conv. / %		C_2 Sel. / %	CO Sel. / %	CO_2 Sel. / %
			CH_4	O_2			
1.5	700	514	0.01	0.7	0.0	100	0.0
3.0	400	525	0.02	0.3	0.0	100	0.0
5.0	200	545	0.01	0.5	0.0	100	0.0
7.0	200	567	0.01	1.2	0.0	100	0.0

[a] CH_4:O_2:Ar = 25:15:60, total flow rate of 100 SCCM; current, 1.5-7.0 mA; catalyst weight, 100 mg; furnace temperature, 423 K.

[b] Catalyst bed temperature measured using a thermocouple.

Table S2. BET surface area of various catalysts as made and after reaction with electric field

Catalyst	BET surface area / $m^2\ g^{-1}$	
	As-made	After reaction
$La_2(WO_4)_3$	1.3	0.4
$Ce_2(WO_4)_3$	1.0	0.7

Table S3. Lattice parameter and band gap of $Ce_2(WO_4)_3$

	U term		lattice parameter				Band gap / eV
	orbital	U_{eff} / eV	a / Ang.	b / Ang.	c / Ang.	β / degree	
Exp.[6,7]		-	7.81	11.7	11.6	109.4	1.64-2.05
Calc.	Ce 4*f* [a)]	0.0	7.92	11.9	11.6	109.2	-
		1.0	7.95	11.9	11.7	109.4	0.78
		2.0	7.96	11.9	11.7	109.4	1.37
		3.0	7.97	12.0	11.7	109.4	1.53
		3.5	7.96	12.0	11.8	109.7	1.82
		4.0	7.97	12.0	11.7	109.3	2.49
		4.5	7.99	12.0	11.7	109.1	2.68
		5.0	7.98	12.0	11.8	109.6	(2.89)
	W 5*d* [b)]	1.0	7.98	12.0	11.8	109.8	1.87
		2.0	7.99	12.0	11.7	109.5	1.95

a) U_{eff} to W 5*d* = 0 eV.

b) U_{eff} to Ce 4*f* = 3.5 eV.

Table S4. Lattice parameter and band gap of $La_2(WO_4)_3$

	U term		lattice parameter				Band gap / eV
	orbital	U_{eff} / eV	a / Ang.	b / Ang.	c / Ang.	β / degree	
Exp.[8]	-	-	7.87	11.8	11.7	110.1	-
Calc.	La 4*f*	0.0	8.00	12.0	11.8	110.2	3.67
		2.0	8.01	12.0	11.8	110.1	3.67
		4.0	8.02	12.1	11.9	110.3	3.66
		6.0	8.03	12.1	11.9	110.2	3.66

U_{eff} to W 5*d* = 0 eV.

Table S5. Effects of charging on various W-O bond lengths and Ce-O bond lengths in the simulated cluster model of (130) facets of $Ce_2(WO_4)_3$ structure

	Bond length / Å	
	Neutral	+1
Ce−O	2.54	2.50
	2.23	2.18
	2.37	2.34
	2.45	2.45
W−O	1.78	1.79
	1.85	1.86
	1.85	1.86
	1.86	1.89

Table S6. Results of Bader charge analyses

	neutral	+8 adiabatic	Δ
Ce	2.25	2.61	0.36
W1	4.34	4.37	0.03
W2	4.41	4.45	0.04
O1	-1.48	-1.39	0.09
O2	-1.45	-1.36	0.09
O3	-1.48	-1.34	0.14
O4	-1.47	-1.37	0.10
O5	-1.44	-1.36	0.07
O6	-1.51	-1.42	0.08

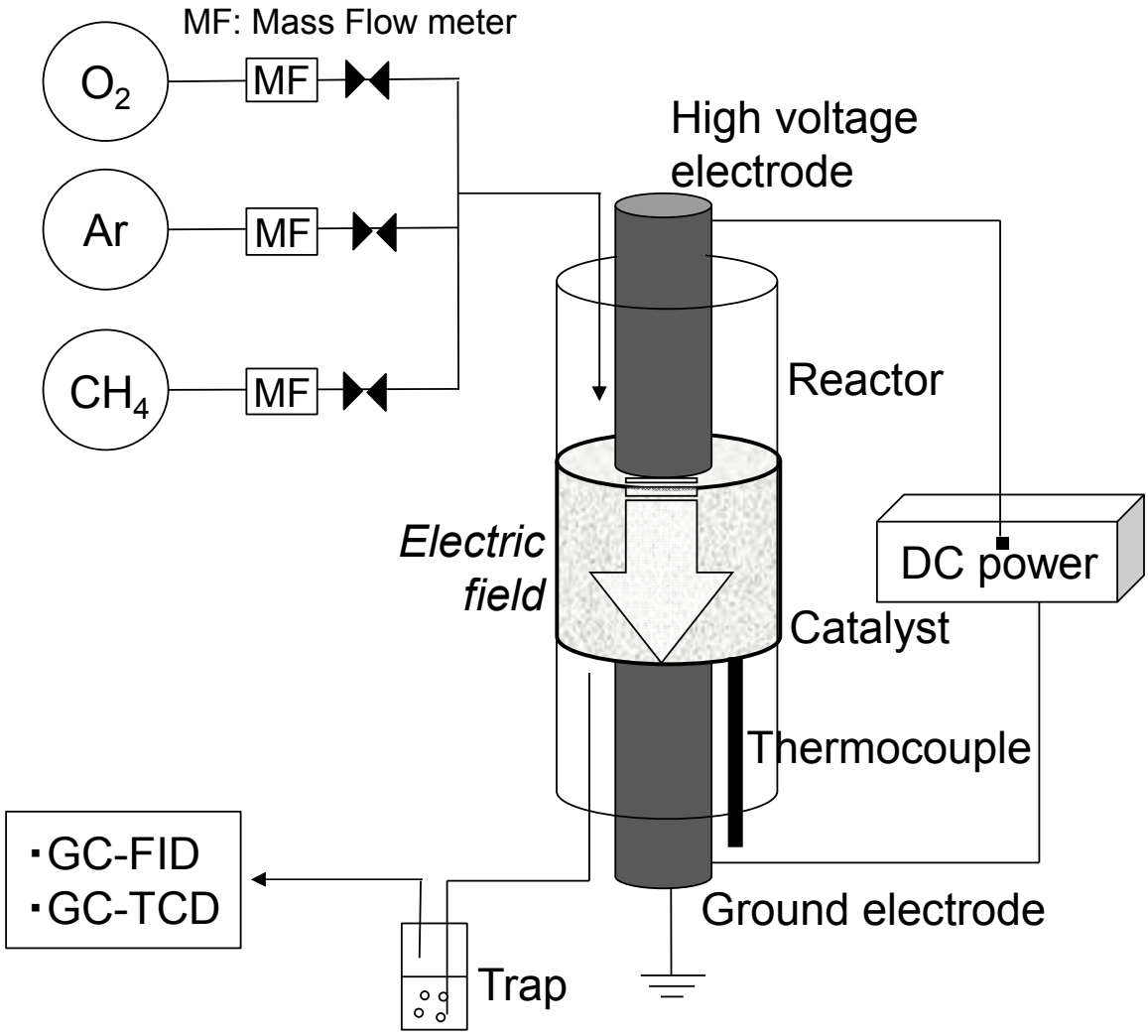

Figure S1. Schematic diagram of reactor for activity test.

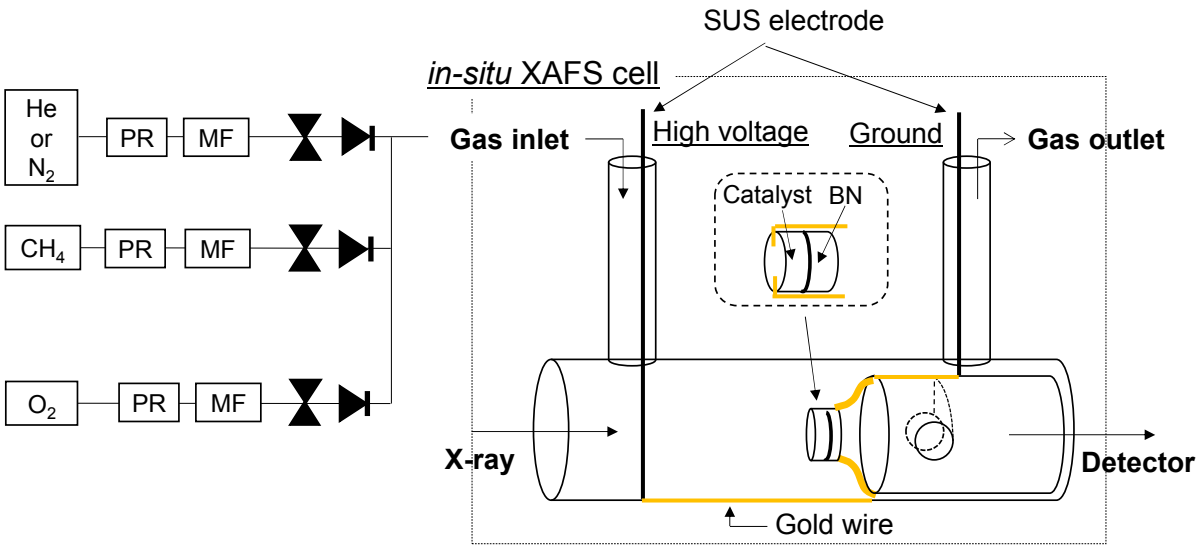

Figure S2. Schematic diagram of reactor for *in-situ* XAFS.

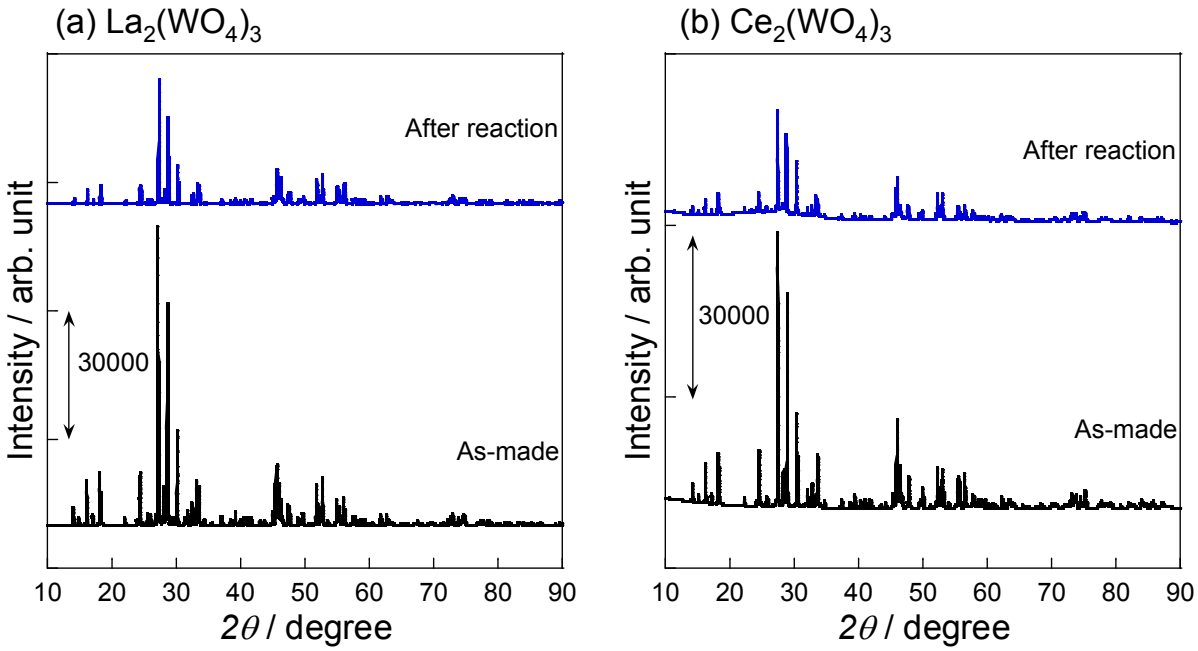

Figure S3. XRD patterns of (a) $La_2(WO_4)_3$ and (b) $Ce_2(WO_4)_3$ catalysts before and after used for oxidative coupling of methane in the electric field.

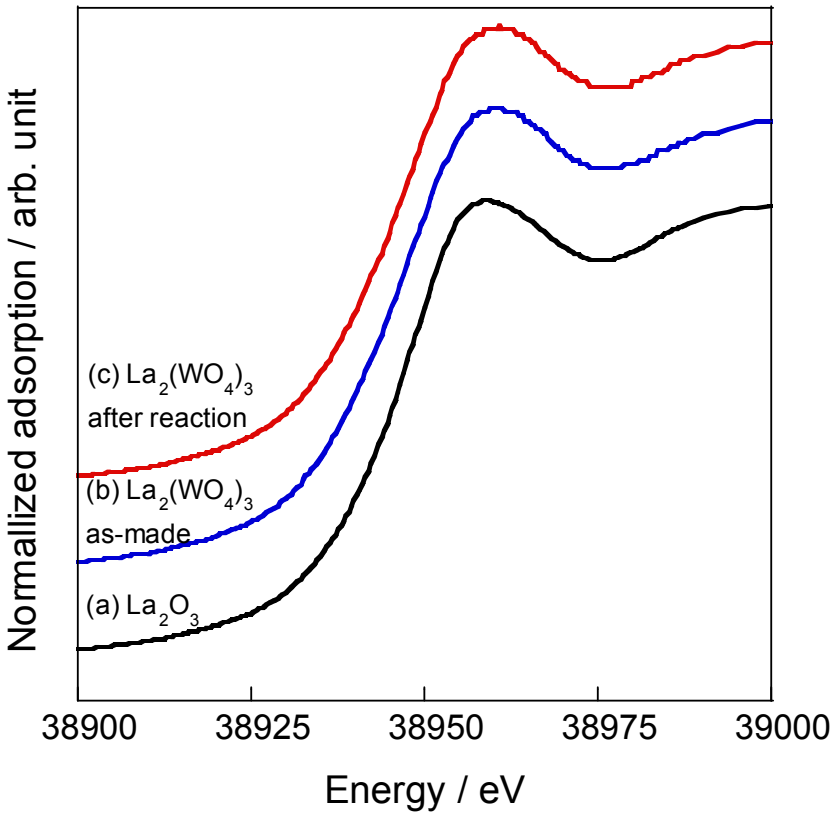

Figure S4. *Ex-situ* La *K*-edge XANES spectra of (a) La_2O_3, (b) $La_2(WO_4)_3$ as-made, and (c) $La_2(WO_4)_3$ after reaction with the electric field.

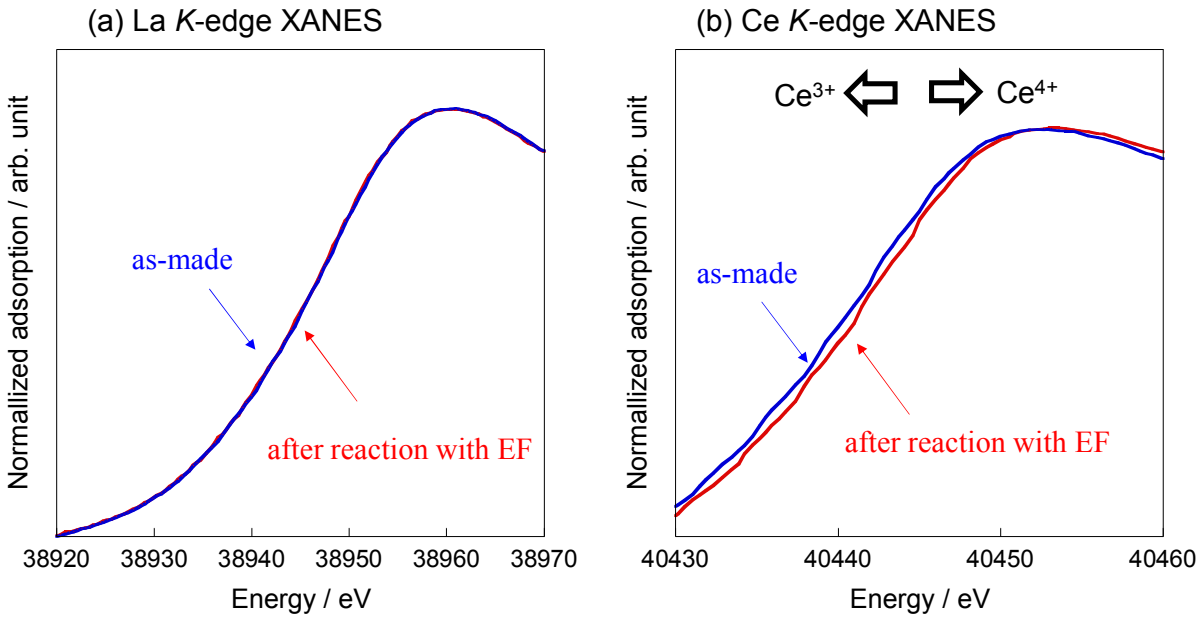

Figure S5. *Ex situ* (a) La *K*-edge and (b) Ce *K*-edge XANES spectra of $La_2(WO_4)_3$ and $Ce_2(WO_4)_3$: (blue line) as-made, (red line) after reaction with EF.

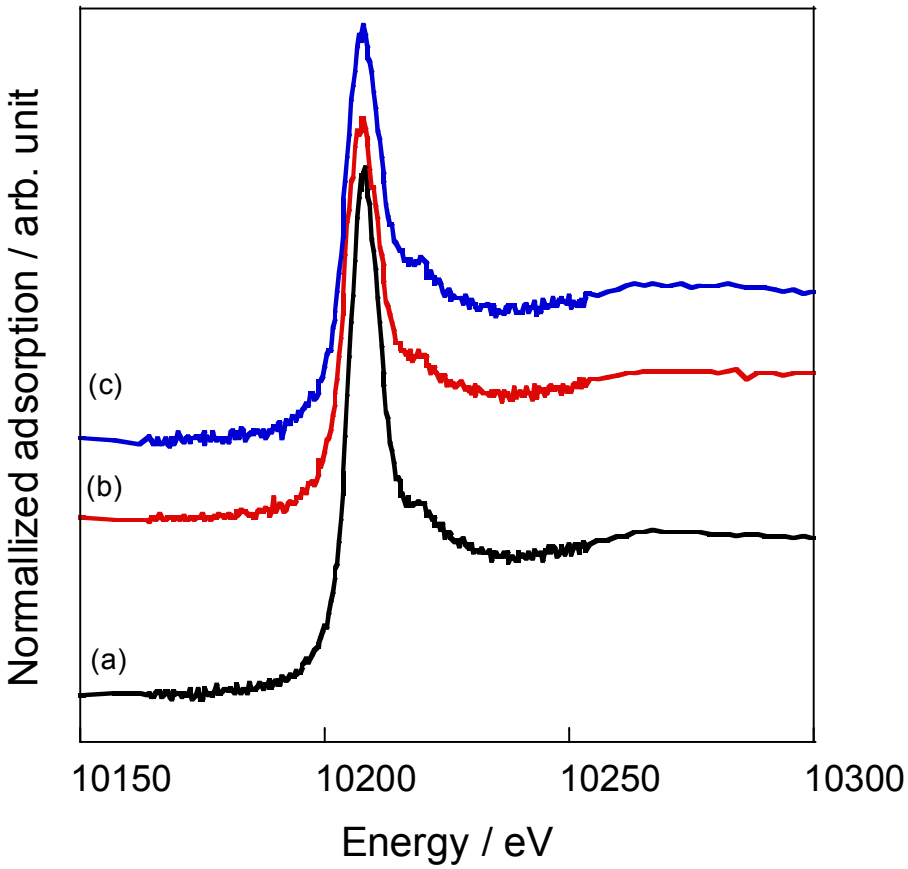

Figure S6. *In-situ* W L_3-edge XANES spectra of $Ce_2(WO_4)_3/CeO_2$ during OCM reaction at 423 K: (a) without EF in $CH_4 + O_2$ flow, (b) with EF (10 mA, 660 V) in $CH_4 + O_2$ flow, (c) without EF after (b).

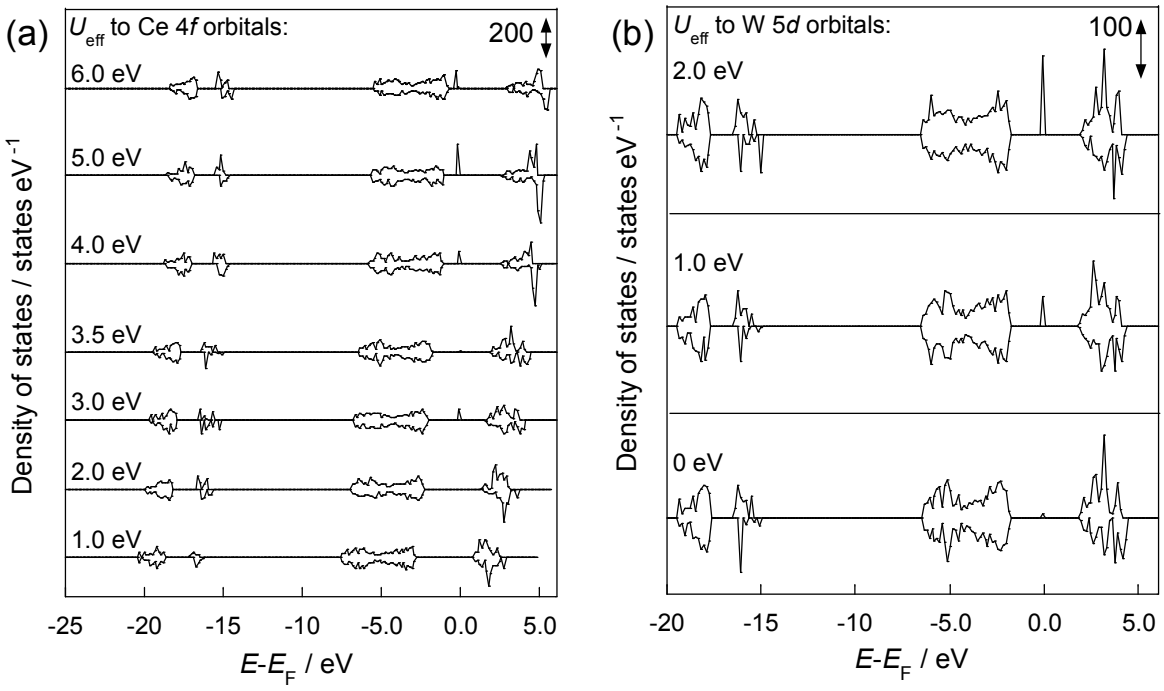

Figure S7. Calculated density of states for $Ce_2(WO_4)_3$: (a) adopting U_{eff} only to Ce 4*f* orbitals (W 5*d* is not adopted U_{eff}), (b) with different U_{eff} to W 5*d* orbitals (U_{eff} = 3.5 eV to Ce 4*f* orbitals is adopted).

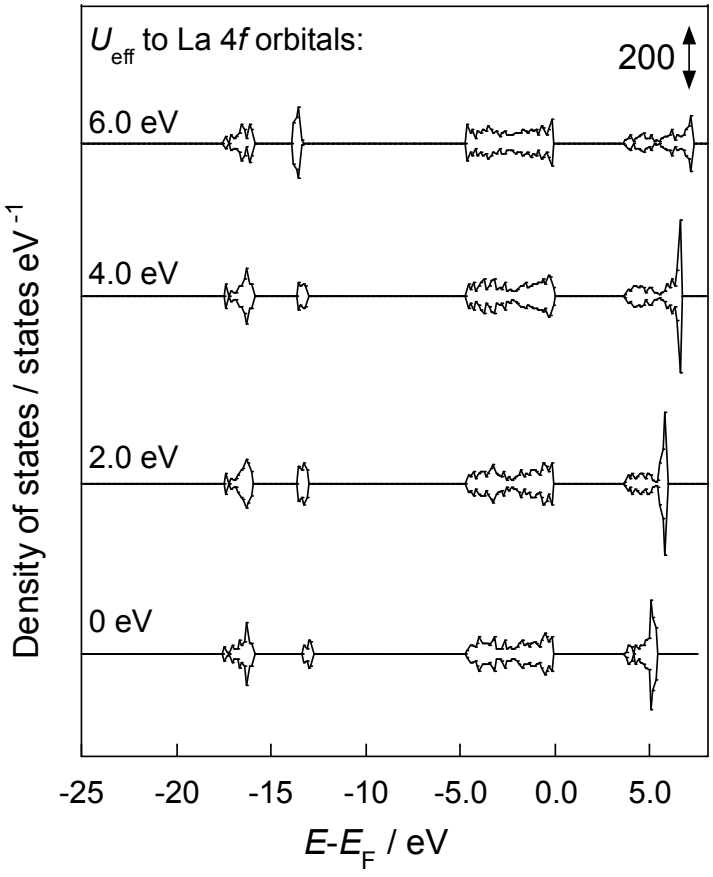

Figure S8. Calculated density of states for $La_2(WO_4)_3$: adopting U_{eff} only to La 4*f* orbitals (W 5*d* is not adopted U_{eff}).

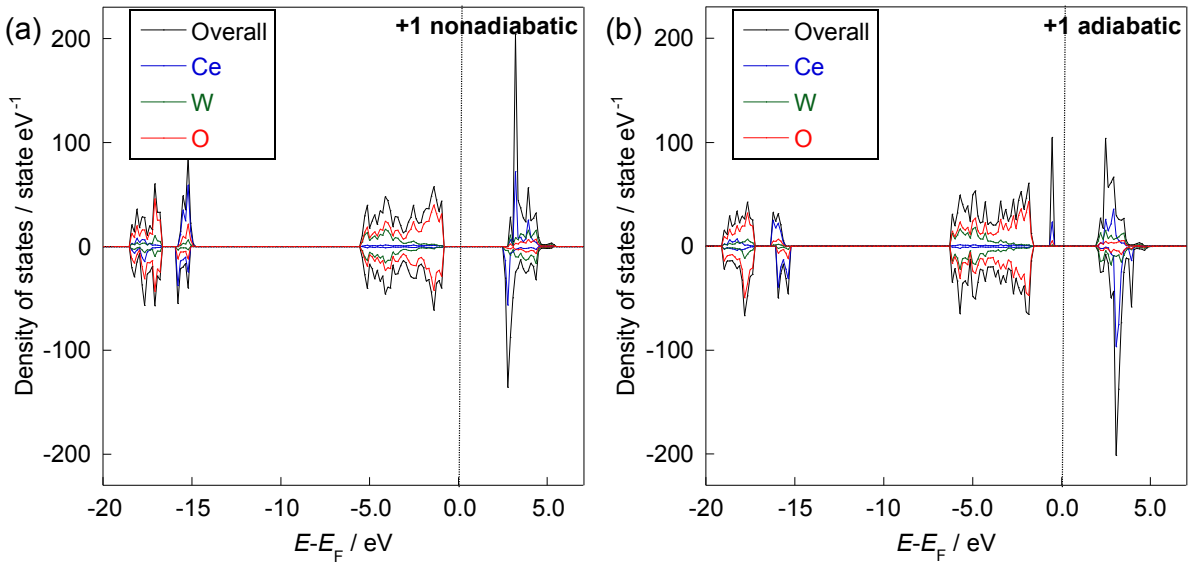

Figure S9. Calculated density of states for $Ce_2(WO_4)_3$ with +1 charged system: (a) without optimization (nonadiabatic) and (b) with optimization (adiabatic).

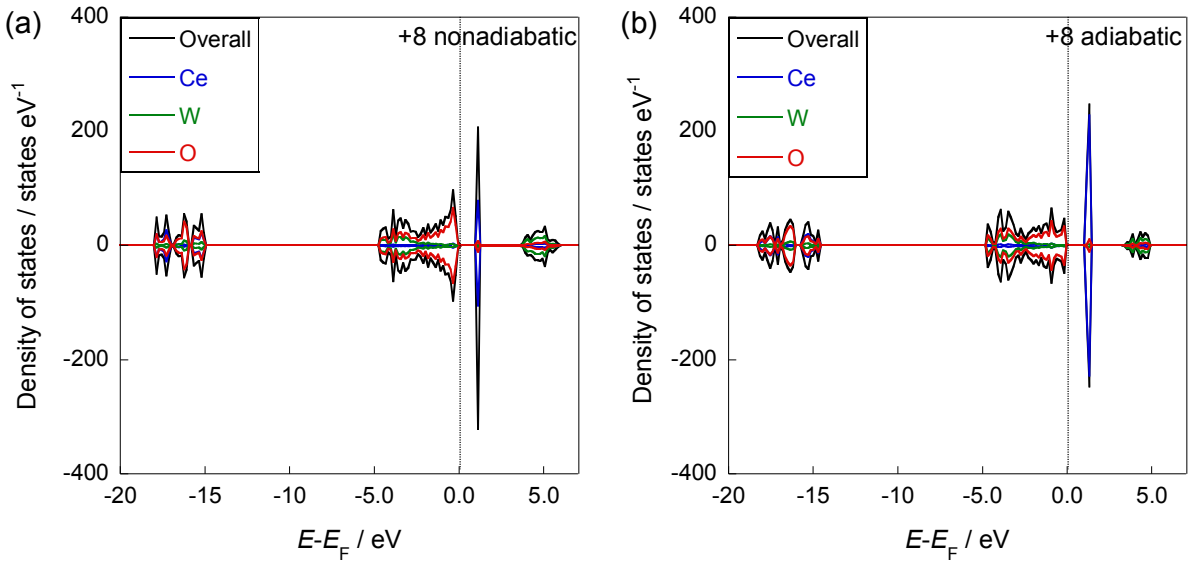

Figure S10. Calculated density of states for $Ce_2(WO_4)_3$ with +8 charged system: (a) without optimization (nonadiabatic) and (b) with optimization (adiabatic).

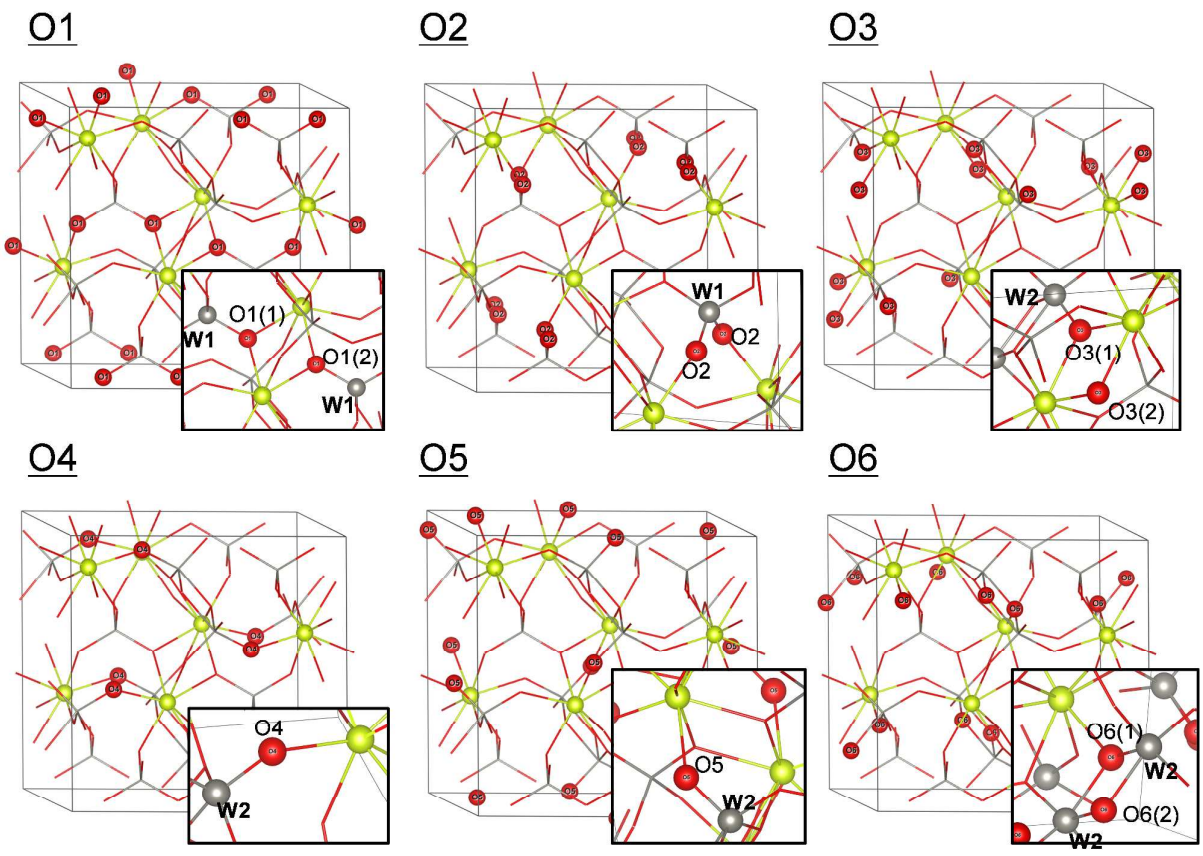

Figure S11. Six kinds of oxygens with different configuration in $Ln_2(WO_4)_3$: (Yellow) Ce or La, (Grey) W, (Red) O.

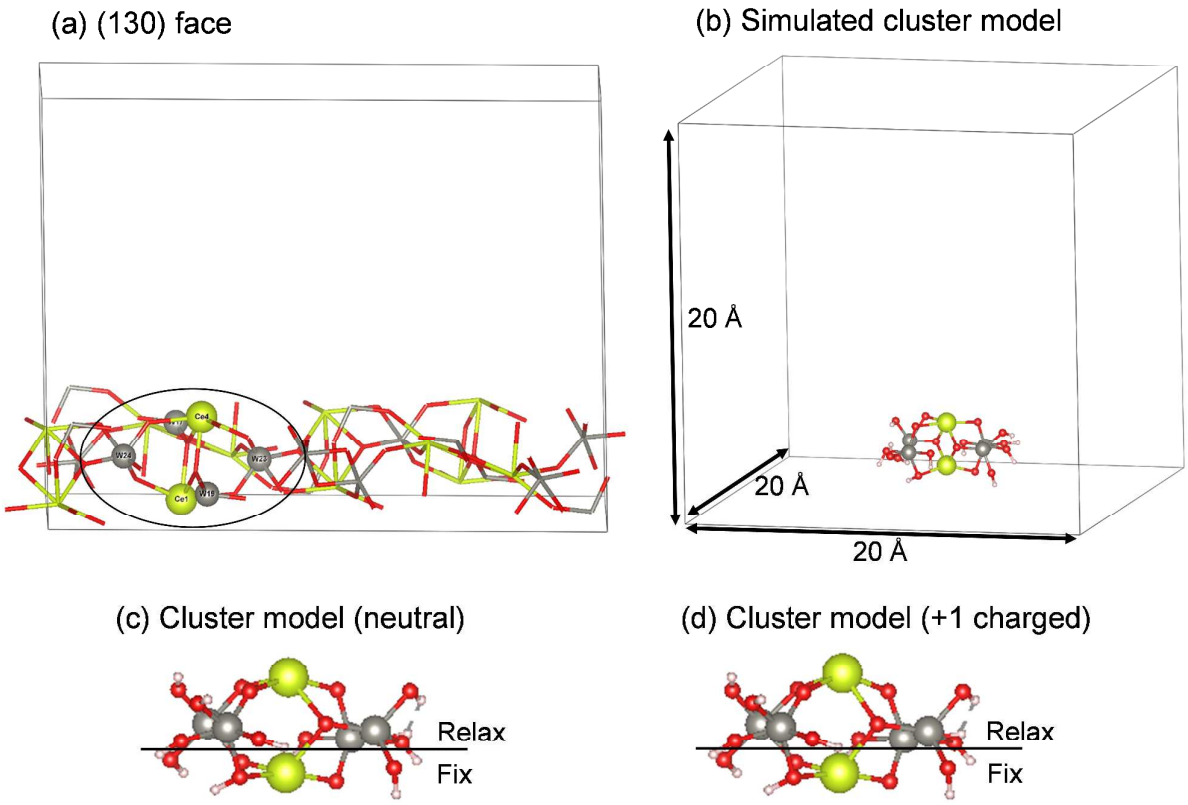

Figure S12. The structure model of $Ce_2(WO_4)_3$: (a) (130) face, (b) simulated cluster model, (c) enlarged cluster model without the electric field (neutral), (d) enlarged cluster model with the electric field (+1 charged). Black circle in (a) were used for simulation of the cluster model.

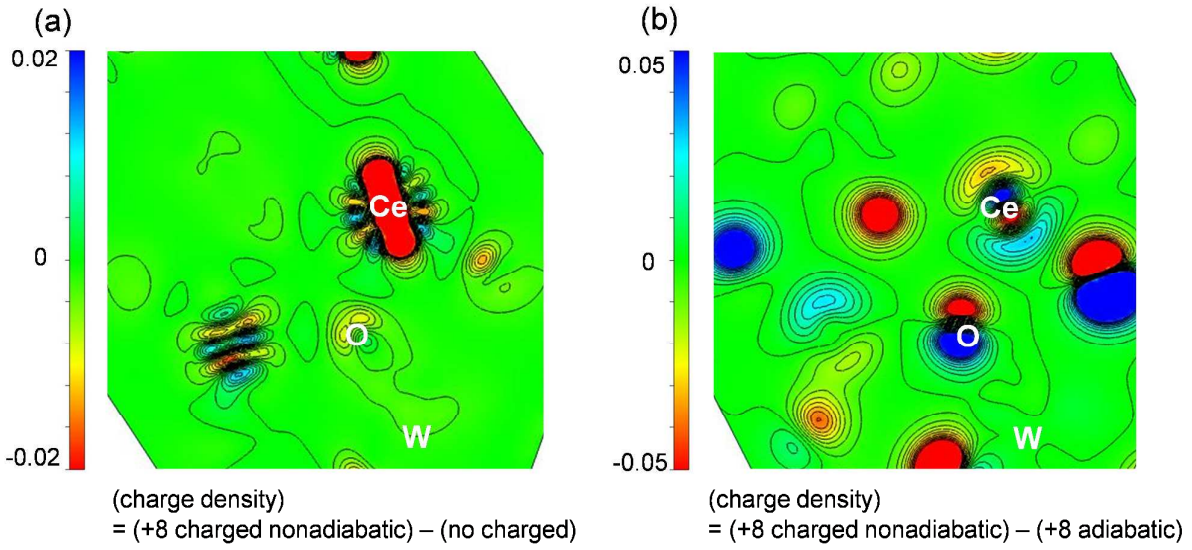

Red region: Electron exists when the system is non-charged, and electron disappears when the system is +8 charged without relaxation (nonadiabatic).

Red region: Electron does not exist when the system is +8 charged without relaxation (nonadiabatic), and electron appears when the system is +8 charged with relaxation (adiabatic).

Figure S13. Charge density difference plots of $Ce_2(WO_4)_3$ around O1(1): (a) (+8 charged without structural relaxation) – (neutral), (b) (+8 charged without structural relaxation) – (+8 with structural relaxation).

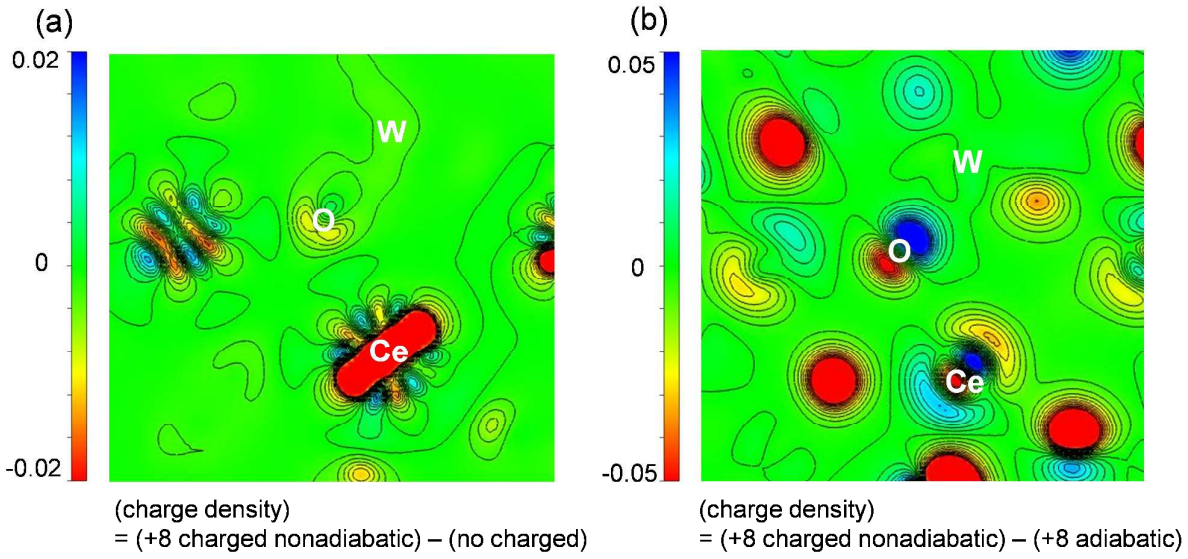

Red region: Electron exists when the system is non-charged, and electron disappears when the system is +8 charged without relaxation (nonadiabatic).

Red region: Electron does not exist when the system is +8 charged without relaxation (nonadiabatic), and electron appears when the system is +8 charged with relaxation (adiabatic).

Figure S14. Charge density difference plots of $Ce_2(WO_4)_3$ around O1(2): (a) (+8 charged without structural relaxation) – (neutral), (b) (+8 charged without structural relaxation) – (+8 with structural relaxation).

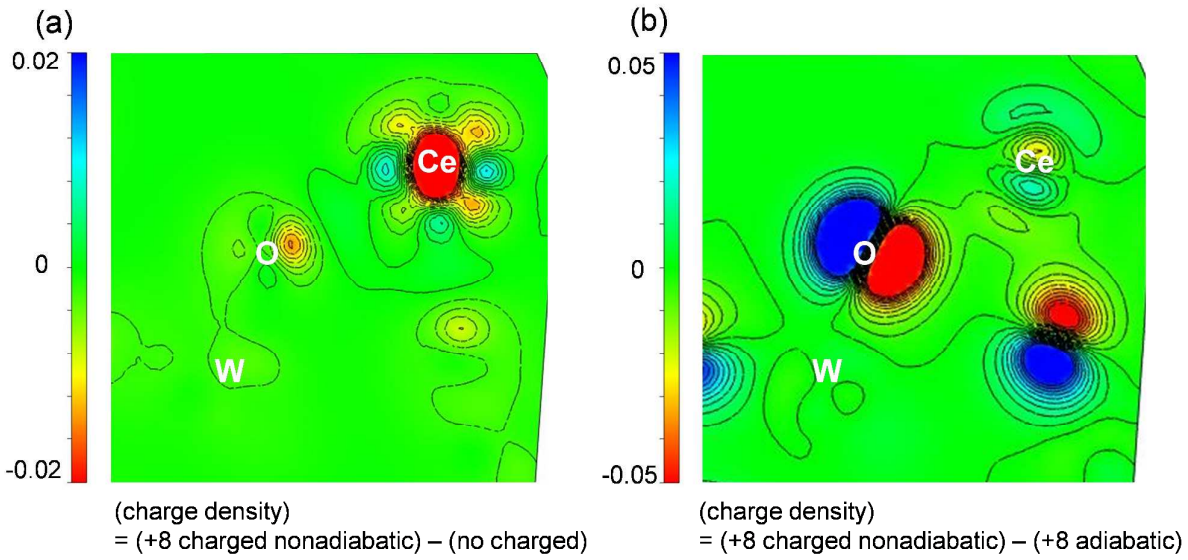

Red region: Electron exists when the system is non-charged, and electron disappears when the system is +8 charged without relaxation (nonadiabatic).

Red region: Electron does not exist when the system is +8 charged without relaxation (nonadiabatic), and electron appears when the system is +8 charged with relaxation (adiabatic).

Figure S15. Charge density difference plots of $Ce_2(WO_4)_3$ around O2: (a) (+8 charged without structural relaxation) – (neutral), (b) (+8 charged without structural relaxation) – (+8 with structural relaxation).

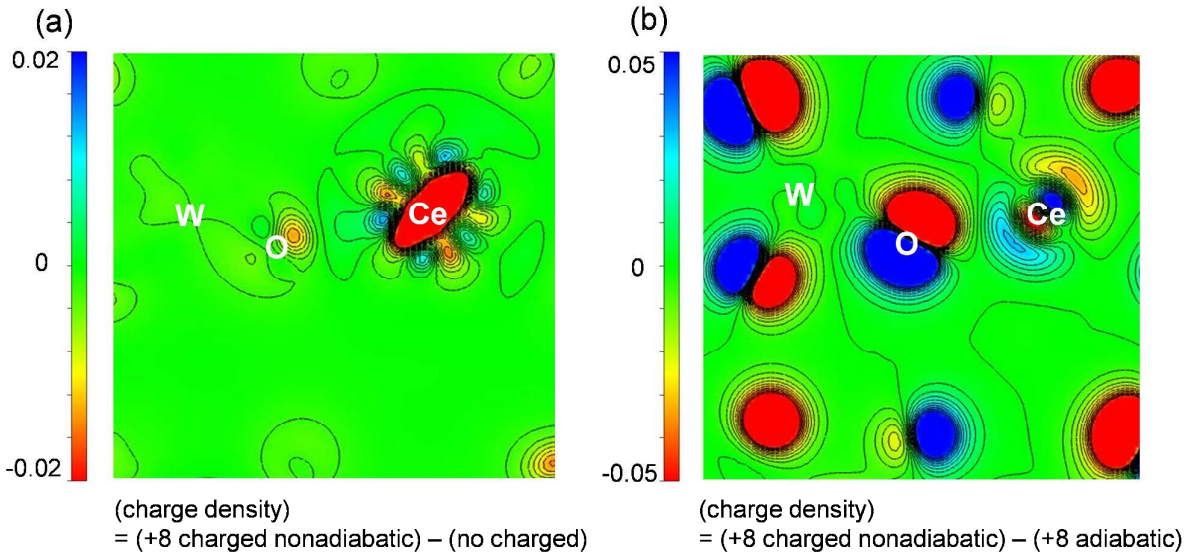

Red region: Electron exists when the system is non-charged, and electron disappears when the system is +8 charged without relaxation (nonadiabatic).

Red region: Electron does not exist when the system is +8 charged without relaxation (nonadiabatic), and electron appears when the system is +8 charged with relaxation (adiabatic).

Figure S16. Charge density difference plots of $Ce_2(WO_4)_3$ around O4: (a) (+8 charged without structural relaxation) – (neutral), (b) (+8 charged without structural relaxation) – (+8 with structural relaxation).

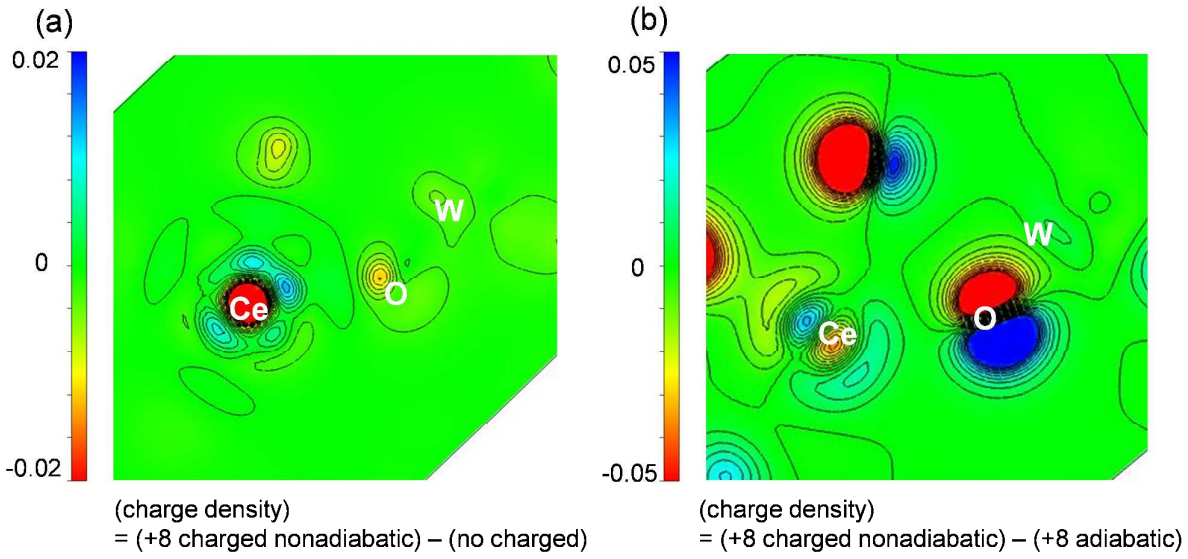

Red region: Electron exists when the system is non-charged, and electron disappears when the system is +8 charged without relaxation (nonadiabatic).

Red region: Electron does not exist when the system is +8 charged without relaxation (nonadiabatic), and electron appears when the system is +8 charged with relaxation (adiabatic).

Figure S17. Charge density difference plots of $Ce_2(WO_4)_3$ around O5: (a) (+8 charged without structural relaxation) – (neutral), (b) (+8 charged without structural relaxation) – (+8 with structural relaxation).

References

(1) Arab, M.; Lopes-Moriyama, L.; dos Santos, T. R.; de Souza, C. P.; Gavarri, J. R.; Leroux, C. Strontium and Cerium Tungstate Materials $SrWO_4$ and $Ce_2(WO_4)_3$: Methane Oxidation and Mixed Conduction. *Catal. Today*. **2013**, *208*, 35−41.

(2) Lopes, F. W. B.; Arab, M.; Macedo, H. P.; de Souza, C. P.; de Souza, J. F.; Gavarri, J. R. High Temperature Conduction and Methane Conversion Capability of $BaCeO_3$ Perovskite. *Powder Technol*. **2013**, *219*, 186–192.

(3) Burcham, L. J.; Wachs, I. E. Vibrational Analysis of the Two Non-Equivalent, Tetrahedral Tungstate (WO_4) Units in $Ce_2(WO_4)_3$ and $La_2(WO_4)_3$. *Spectrochimica Acta A*. **1994**, *54*, 1355−1368.

(4) Sugiura, K.; Ogo, S.; Iwasaki, K.; Yabe, T.; Sekine, Y. Low-Temperature Catalytic Oxidative Coupling of Methane in an Electric Field Over a Ce–W–O Catalyst System. *Sci. Rep*. **2016**, *6*, 25154.

(5) Mamede, A.-S.; Payen, E.; Grange, P.; Poncelet, G.; Ion, A.; Alifanti, M.; Pârvulescu, V. I. Characterization of WO_x/CeO_2 Catalysts and Their Reactivity in the Isomerization of Hexane. *J. Catal*. **2004**, *223*, 1–12.

(6) Gressling, T.; Müller-Buschbaum, Hk. Zur Kristallstruktur von $Ce_2(WO_4)_3$. *Z. Naturforsch.* **1995**, *50b*, 1513−1516 (*written in German*).

(7) Sun, B.; Li, X.; Liang, D.; Chen, P. Effect of Visible-Light Illumination on Resistive Switching Characteristics in $Ag/Ce_2W_3O_{12}$/FTO Devices. *Chem. Phys. Lett*. **2016**, *643,* 66−70.

(8) Gärtner, M.; Abeln, D.; Pring, A.; Wilde, M.; Reller, A. Synthesis, Structure, and Reactivity of Novel Lanthanum Tungstates. *J. Solid State Chem*. **1994**, *111*, 128−133.